

**KL edges in x-ray-absorption spectra of third-period atoms: Si, P, S, and Cl**

Adriano Filipponi

*Dipartimento di Fisica, Università degli Studi dell'Aquila, Via Vetoio, 67010 Coppito, L'Aquila, Italy*

Trevor A. Tyson and Keith O. Hodgson

*Department of Chemistry, Stanford University, Stanford, California 94305*

Settimio Mobilio

*Dipartimento di Energetica, Università dell'Aquila, Roio Monte Luco, 67100 L'Aquila, Italy**and Istituto Nazionale di Fisica Nucleare, Laboratori Nazionali di Frascati, Cassella Postale 13, 00044 Frascati, Italy*

(Received 3 December 1992)

A systematic investigation of double-electron *KL*-edge resonances in x-ray-absorption spectra of third-period atoms (Si, P, S, and Cl) is presented. Experimental data on  $\text{NaH}_2\text{PO}_4$ , Graham's salts ( $\text{Na}_2\text{O}:\text{P}_2\text{O}_5$ ),  $\text{Na}_4\text{P}_2\text{O}_7$ , elemental S,  $\text{Na}_2\text{SO}_3$ ,  $\text{K}_2\text{SO}_4$ ,  $\text{CuSO}_4$ ,  $\text{Na}_2\text{S}_2\text{O}_3$ ,  $\text{Na}_2\text{S}_2\text{O}_6$ ,  $\text{NaClO}_2$ ,  $\text{NaClO}_3$ , and  $\text{NH}_4\text{ClO}_4$  are reported and discussed in combination with previous measurements at the Si *KL* edge of  $\text{SiX}_4$ , ( $X = \text{H}, \text{CH}_3, \text{Br}, \text{Cl}, \text{F}$ ) molecules. The further comparison of these results with *KL*-edge structures in Ne and Ar provides an almost complete overview of these excitations for third-period atoms. A compilation of energies and oscillator strengths for the dominant resonances is reported and the main trends of energy splitting, intensity, and energy position versus oxidation state and *Z* number are discussed.

PACS number(s): 32.30.Rj, 32.70.Jz, 78.70.Dm

**I. INTRODUCTION**

Multielectron excitation effects in x-ray absorption spectra are the subject of renewed interest in both fundamental and applied fields. The relaxation of the charge distribution following a single-electron excitation process may induce a further internal excitation of the atomic charge. In terms of a one-electron scheme, processes involving the excitation of two or more electrons can occur with decreasing amplitude. For the dominant multielectron processes, involving two electrons, one may distinguish between three kinds of configurations which accompany the main single-electron excitation channels. These are (a) the discrete resonances with the two excited electrons in discrete, previously unoccupied orbitals; (b) the shake-up channels in which one of these two electrons is in the continuum; and (c) the shake-off configurations in which both electrons are excited into continuum states. All these configurations contribute to the photon absorption cross section; however, the main features are expected to arise from discrete resonances and the associated shake-up channels because of their sudden onset. The importance of understanding these shake phenomena cannot be overemphasized. Multielectron excitation features are a direct manifestation of correlation effects among the electrons and consequently their investigation covers fundamental aspects of atomic physics.

Early examples for multielectron excitation effects in x-ray absorption spectra were the observations of the Kr *LN* edges [1] and the Ar *KM* edge [2]. The Ar *KM* resonances have been, more recently, the subject of careful investigations involving also measurements of the fluorescence and Auger decays of the excited states [3,4]. Several investigations, over the past decade, have been

carried out at the *K* edge of Kr where evidence for the presence of the *KN*<sub>1</sub>, *KM*<sub>4,5</sub>, and *KM*<sub>2,3</sub> edges is found [5–7]. Recently the same features have been identified above the Br *K* edge in spectra of HBr and Br<sub>2</sub> [8]. In the Kr and Br cases the channel onsets are mainly associated with a slope change of the absorption coefficient departing from the smooth one-electron atomic background. Further evidence for background slope changes has been observed at the *L* edges [9] and *K* edge [10] of Xe.

In condensed phases the identification of double-electron excitation features is hampered by the presence of the structural oscillations referred to as the extended x-ray absorption fine structure (EXAFS) [11]. The EXAFS and the atomic background, containing steps and slope changes associated with multielectron edges, are interwoven, resulting in a complex total cross section from which it is difficult to extract the pure structural signal. Nevertheless, wide evidence for the effects of the shake-up channels in condensed systems was found. The *KL* edge of Si was first identified in amorphous silicon (*a*-Si:H) spectra [12] and subsequently revealed in  $\text{SiX}_4$  ( $X = \text{H}, \text{CH}_3, \text{Br}, \text{Cl}, \text{F}$ ) molecules [13,14]. Several other examples have been discovered involving different elements. In rare-earth compounds, a structure with width approximately twice that of main line and corresponding to the  $4d \rightarrow 5d$  shake-up transition is seen [15]. This feature has been found to be even more evident in magnetic circular x-ray dichroism spectra [16]. A new method for isolating the atomic background contribution based on an iterative procedure was proposed in a recent letter [17] and applied to RbBr, where the *KM*<sub>4,5</sub> edges of Rb and Br were seen, and to PbO<sub>2</sub> where evidence for additional excitations of *4f* electrons was found. This overview makes it clear that the occurrence of multiple-excitation features

in absorption spectra is rather general.

Clearly, multiple excitation effects can be probed by other spectroscopies. X-ray photoemission spectroscopy allows one to identify the main possible rearrangement of the passive atomic shells which produce shake-up satellites of the main core peaks, but unfortunately does not allow access to the discrete excitation region. In Auger and fluorescence spectroscopies, extra satellites associated with the double-hole decay are expected, but the analysis of the spectra is usually difficult due to the large number of possible decay channels. Consequently, x-ray absorption spectroscopy is a particularly suitable technique to study double-electron discrete resonances.

Discrete resonances associated with the formation of two core holes were observed only in a limited number of cases. They are degenerate with several continua and for this reason undergo an autoionization phenomenon that may contribute to their intrinsic width and produce an asymmetric line shape [18]. The discrete autoionizing resonances of He [19] near 60 eV were the first examples of double-electron excitations observed in the absorption coefficient of atoms. In this case, however, only weakly bound electrons belonging to the same  $1s$  shell are involved. To date, the most evident double-electron discrete resonances following a true deep core-level threshold have been observed in the case of Ne [20],  $\text{SiX}_4$  molecules [13], and very recently Ar [21], involving both the  $1s$  and the  $2p$  electrons ( $KL$  edge). Failures to observe the  $KL$  edge in transition metals were explained by the presence of the open  $3d$  shell producing a large number of  $^1P$  terms spread over a wide energy range [22]. These results suggest that the  $KL$  edge is a peculiar feature of Ne and third-period atoms.

In this paper we present a systematic investigation of these  $KL$ -edge resonances showing the results of experiments performed at two synchrotron-radiation facilities on many P, S, and Cl compounds which reveal the presence of very intense features in solid-phase systems. The presentation includes previously published data at the Si  $K$  edge [13] and comparisons with the Ne [20] and Ar [21] results.

The interpretation of these one-photon, many-electron processes forces one to go beyond the one-electron approximation and to include correlation effects in order to account for the observed multiplet splitting, line intensities, and autoionizing shapes. This occurrence explains the basic atomic-physics interest in this subject of research.

This paper is organized as follows. In Sec. II the experimental details are discussed and the whole set of experimental data is presented. Section III is devoted to the interpretation of the results and emphasis is given to the experimental trends versus atomic number and oxidation state. It is divided into two parts: the first contains mainly the discussion of the energy positions of the resonances and the second deals with peak intensities and profiles.

## II. EXPERIMENT

The experiments were carried out in parallel at the Frascati and Stanford synchrotron radiation facilities.

High-purity commercial salts were used to produce samples suitable for absorption or fluorescence measurements. Below are reported the experimental details with a description of the observed spectra.

### A. Experimental details for Frascati measurements

Measurements of samples of  $\text{NH}_4\text{ClO}_4$ ,  $\text{NaClO}_3$ ,  $\text{NaClO}_2$ , elemental S,  $\text{Na}_2\text{SO}_3$ ,  $\text{K}_2\text{SO}_4$ ,  $\text{NaH}_2\text{PO}_4$ ,  $\text{Na}_2\text{O:P}_2\text{O}_5$ , and  $\text{Na}_4\text{P}_2\text{O}_7$  were performed at the Frascati synchrotron radiation PULS Facility. The EXAFS beamline was equipped with a Si(111) channel-cut monochromator. The Adone storage ring was operating at 1.3 GeV under specific request to reduce higher-order harmonics in the monochromatized beam. Several spectra were obtained at the Cl, S, and P edges of the various compounds.

In order to produce samples of an appropriate thickness for absorption studies the salts were finally ground with a mortar and the powder was poured into a nonsolvent liquid. The suspension was allowed to settle for some time in such a way that the largest particles came out of the suspension. The suspension was then filtered through a Millipore polycarbonate membrane. By this procedure, a rather uniform layer of powder was obtained. The thickness of the sample was chosen in order to obtain the best signal-to-noise ratio in absorption measurements. The polycarbonate substrate material absorbed a negligible amount of x-ray radiation over the energy range being studied.

Some spectra were taken over a full energy range to include the  $K$  and  $KL$  edges, while other scans were taken with a finer energy spacing only in the  $KL$ -edge region. The phosphorus  $K$  edge at about 2149 eV lies below the minimum energy reachable with the Si(111) monochromator; however, the  $KL$ -edge region could be observed. The energy calibration of the spectra was performed by setting the energy of the first peak maximum at the Ar  $K$  edge, corresponding to the  $1s \rightarrow 4p$  transition, to 3203.3 eV.

### B. Experimental details for Stanford measurements

The S  $K$ -edge spectra of  $\text{CuSO}_4$ ,  $\text{Na}_2\text{S}_2\text{O}_3$ , and  $\text{Na}_2\text{S}_2\text{O}_6$  were measured at the Stanford Synchrotron Radiation Laboratory using the SSRL-Exxon-LBL 54-pole wiggler beamline 6-2 operated in undulator mode at 3.0 GeV (see Ref. [23] for more details on the experimental setup). The spectra were recorded not by direct absorption but by measurement of the x-ray-fluorescence decay of the samples excited with the incident x-ray beam. A monochromator composed of a pair of Si(111) crystals was used and higher harmonics were minimized by detuning the crystals (i.e., making them slightly nonparallel). Energy calibration was carried out by defining the energy of the maximum of the first peak in a calibration sample of  $\text{Na}_2\text{S}_2\text{O}_3 \cdot 2\text{H}_2\text{O}$  to be 2472.0 eV.

The spectra of samples of  $\text{CuSO}_4$ ,  $\text{Na}_2\text{S}_2\text{O}_3$ , and  $\text{Na}_2\text{S}_2\text{O}_6$  were measured on the compounds:  $\text{CuSO}_4 \cdot 5\text{H}_2\text{O}$ ,  $\text{Na}_2\text{S}_2\text{O}_3 \cdot 2\text{H}_2\text{O}$ , and  $\text{Na}_2\text{S}_2\text{O}_6 \cdot 5\text{H}_2\text{O}$ . These samples (as well as the calibration sample) were prepared as finely ground powders and distributed uni-

formly on Mylar tape. For each sample, several scans in energy covering the *K*- and *KL*-edge regions were averaged to produce the spectra presented here.

### C. Observed spectra

The spectra presented in the following figures are scaled in amplitude to have a unitary edge jump. The jump (*J*) is defined as the difference in absorption of the extrapolation of fits of the pre-edge background and of the post-edge spectrum using appropriate functional forms at the threshold energy. The threshold is defined as the first inflection point before the first discrete resonance at the *K* edge [referred to as main line ML in the following]. Herein we report experimental data concerning the *K* and *KL* edges in order of decreasing *Z* number.

The Cl *K* edges of NaClO<sub>2</sub>, NaClO<sub>3</sub>, and NH<sub>4</sub>ClO<sub>4</sub> are reported in Fig. 1. The threshold energy region is dominated by the presence of a very intense discrete resonance (ML) corresponding to the transition  $1s \rightarrow 3p^*$  ( $3p^*$  indicates the first symmetry-allowed unoccupied resonance), followed by a strong near-edge structure. The relative ML energy position of the three spectra is real and reflects the increase of photon energy required for the  $1s \rightarrow 3p^*$  transition. Such effect is related to the increase of the binding energy of the  $1s$  core electron and the oxidation state of the absorber and will be referred to as chemical shift in the following discussion.

The NaClO<sub>2</sub> samples were prepared with special care because the compound is not stable and is easily oxidized by reaction with water. The deposition procedure was performed in a dry-box and the sample was exposed to air only for a few seconds to make the transfer from the dry-box to the sample chamber of the beamline that was then immediately evacuated to about  $10^{-5}$  Torr. The NaClO<sub>2</sub>

sample, however, was slightly contaminated by ClO<sub>3</sub><sup>-</sup> anions by an amount of about 10% as evidenced by the small peak following the ML in the sample. This small peak coincides in energy with that from the NaClO<sub>3</sub> ML. This contamination does not affect the *KL*-edge results.

In the spectrum of NH<sub>4</sub>ClO<sub>4</sub> a broad feature with a half width at half maximum (HWHM) of approximately 5 eV can be seen after the ML. This one-electron feature, called a shape resonance, can be explained classically as the "trapping" of the photoelectron partial-wave components by the molecular field [24]. In molecules, in addition to the *l* channel of an exciting wave, the scattered wave can have all *l* channels allowed by the symmetry about absorbing site. The classic example is the N<sub>2</sub> molecule where the *l*=3 exciting wave has a large *l*=1 projection on the absorbing site and one sees a broad structure approximately 15 eV above threshold. We now turn to the two-electron features.

The Cl *KL*-edge region of NaClO<sub>2</sub>, NaClO<sub>3</sub>, and NH<sub>4</sub>ClO<sub>4</sub> is shown in Fig. 2. The energy scale as well as the amplitude is consistent with that given in Fig. 1. These data will be discussed in detail in the following sections, but two major features should be pointed out: (a) the *KL*-edge resonances undergo a chemical shift similar to that occurring at the *K* edge, but of larger magnitude (see also Sec. III A and Table I); and (b) the amplitude of the resonances increases strongly as a function of the oxidation state of Cl, an effect much more evident than the corresponding ML increase at the *K* edge. Notice that the shape of the resonance region and the multiplet structure is very similar going from NaClO<sub>2</sub> to NH<sub>4</sub>ClO<sub>4</sub>, indicating the dominance of atomic character in the observed resonances. Some differences in the NaClO<sub>2</sub> spectrum can be clearly attributed to the NaClO<sub>3</sub> contamination

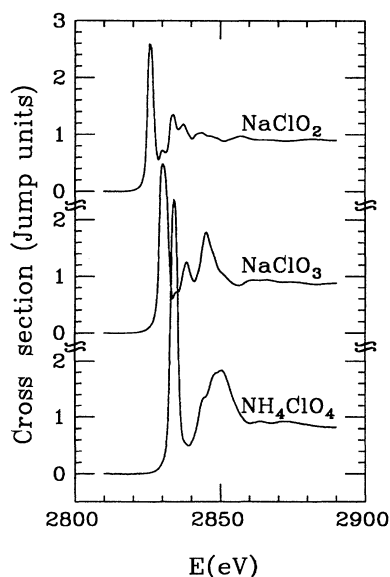


FIG. 1. Cl *K*-edge spectra of NaClO<sub>2</sub>, NaClO<sub>3</sub>, and NH<sub>4</sub>ClO<sub>4</sub>. Notice the intense discrete resonance at the edge and the chemical shifts.

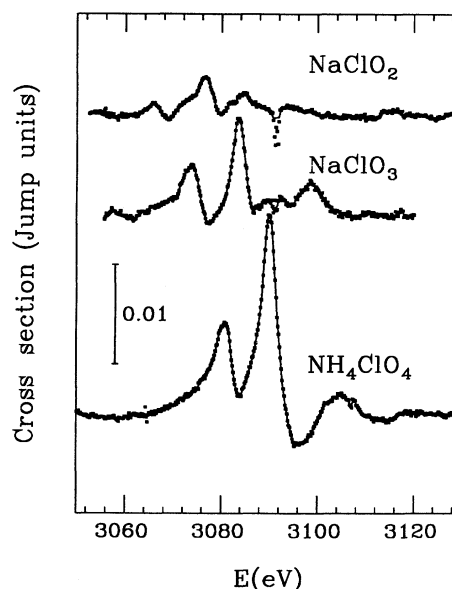


FIG. 2. Cl *KL*-edge spectra of NaClO<sub>2</sub>, NaClO<sub>3</sub>, and NH<sub>4</sub>ClO<sub>4</sub>. Notice the similarities among the various spectra in addition to the energy shift and increase in intensity with increasing formal oxidation state of Cl.

that appears more visible than at the *K* edge because the *KL*-edge resonance cross section is strongly enhanced in  $\text{NaClO}_3$ .

We report the S *K*-edge threshold region for various sulfur compounds including elemental sulfur S,  $\text{Na}_2\text{SO}_3$ , and  $\text{K}_2\text{SO}_4$  in Fig. 3(a) and  $\text{Na}_2\text{S}_2\text{O}_3$ ,  $\text{Na}_2\text{S}_2\text{O}_6$ , and  $\text{CuSO}_4$  in Fig. 3(b). In Fig. 4 the corresponding S *KL*-edge energy regions are presented. The primary shapes and trends are very similar to those occurring in the case of the Cl edge. Finer details of some of the *K*-edge spectra reveal a nontrivial near-edge structure. Some features can be attributed to the more complex molecular structures (like in  $\text{Na}_2\text{S}_2\text{O}_3$  and  $\text{Na}_2\text{S}_2\text{O}_6$ , for instance [23])

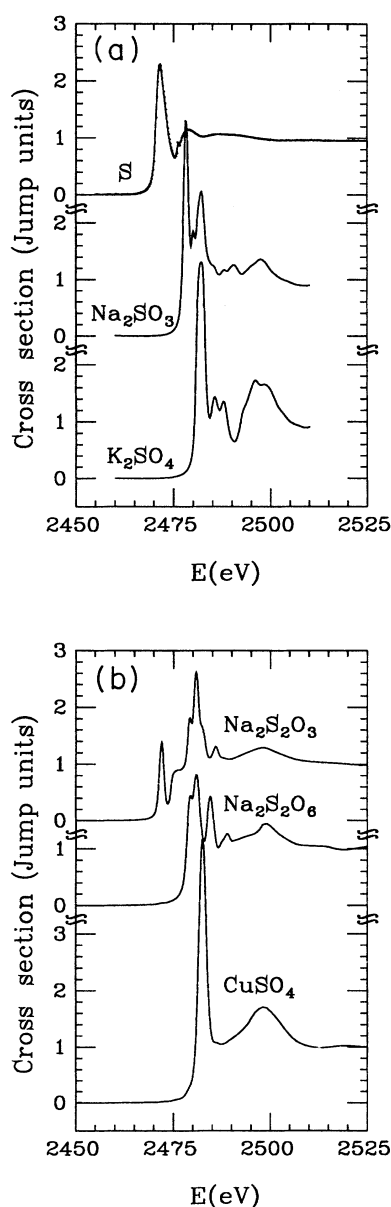


FIG. 3. (a) S *K*-edge spectra of elemental sulfur,  $\text{Na}_2\text{SO}_3$  and  $\text{K}_2\text{SO}_4$ . (b) S *K*-edge spectra of  $\text{Na}_2\text{S}_2\text{O}_3$ ,  $\text{Na}_2\text{S}_2\text{O}_6$ , and  $\text{CuSO}_4$ .

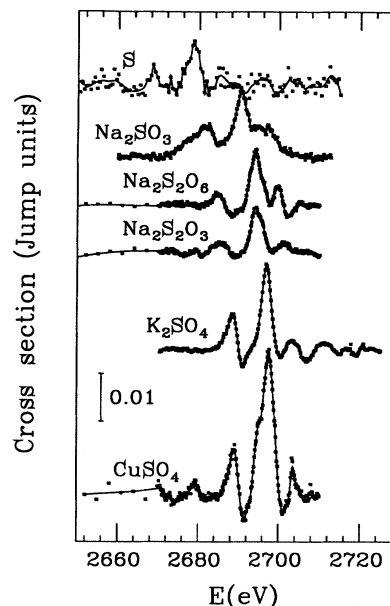


FIG. 4. S *KL*-edge spectra of elemental sulfur,  $\text{Na}_2\text{SO}_3$ ,  $\text{Na}_2\text{S}_2\text{O}_3$ ,  $\text{Na}_2\text{S}_2\text{O}_6$ ,  $\text{K}_2\text{SO}_4$ , and  $\text{CuSO}_4$ . The *KL*-edge shape resembles the Cl data presented in Fig. 2.

while the differences between  $\text{K}_2\text{SO}_4$  and  $\text{CuSO}_4$  are attributed to the different atomic environment beyond the first coordination shell in the two compounds.

The P *KL*-edge spectra of the  $\text{Na}_2\text{O}:\text{P}_2\text{O}_5$ ,  $\text{Na}_4\text{P}_2\text{O}_7$ , and  $\text{NaH}_2\text{PO}_4$  are seen in Fig. 5. In this case the amplitudes could not be calibrated with the relative P *K*-edge jump because the Si(111) monochromator could not reach such a low energy, and therefore no amplitude compar-

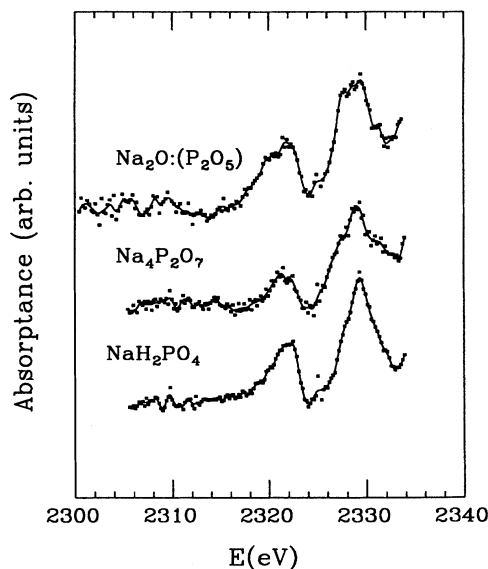


FIG. 5. P *KL*-edge spectra of  $\text{Na}_2\text{O}:\text{P}_2\text{O}_5$ ,  $\text{Na}_4\text{P}_2\text{O}_7$ , and  $\text{NaH}_2\text{PO}_4$ . The overall shape is again very similar to the Cl and S data.

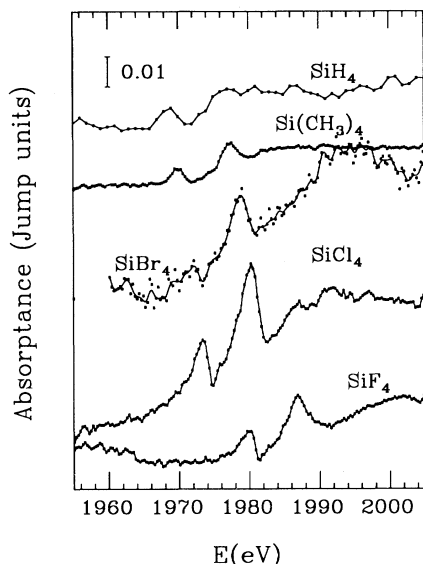


FIG. 6. Previously published [13] Si *KL*-edge spectra of  $\text{SiH}_4$ ,  $\text{Si}(\text{CH}_3)_4$ ,  $\text{SiBr}_4$ ,  $\text{SiCl}_4$ , and  $\text{SiF}_4$ , repeated here for comparison.

ison could be performed. It is, however, reasonable to believe that the maximum relative amplitudes are reached in the case of the  $\text{NaH}_2\text{PO}_4$  compound. The double-peak dominant feature of the *KL* edge is again observed even if the signal-to-noise ratio is not as good as in the measurements described above. The  $\text{Na}_4\text{P}_2\text{O}_7$  and  $\text{NaH}_2\text{PO}_4$  spectra look very similar, as expected due to the similar oxidation states of the P atoms. The spectra of  $\text{Na}_2\text{O:P}_2\text{O}_5$  instead shows flat maxima reminiscent of a mixture of nonequivalent P atoms.

In order to complete the presently available experimental data for resonance peaks at the *KL* edge of third-period atoms, we reproduce in Fig. 6 our previously published results on the Si *KL*-edge features for  $\text{SiX}_4$  ( $X=\text{H}, \text{CH}_3, \text{Br}, \text{Cl}, \text{F}$ ) molecules [13]. Again, the overall evidence for a double-structured peak is clear, as well as the trend of increasing intensity and progressive energy shift of the resonances with increasing electronegativity of the ligands.

### III. RESULTS AND DISCUSSION

The experimental evidence for resonance structures at the *KL* edge of atoms discussed above is made more complete with the previously mentioned measurements of the Ne [20] and Ar [21] *KL* edges. Thus besides Ne, which is the first element in which the  $2p$  electrons can reasonably be considered core states, the *KL* edge has been identified in Si, P, S, Cl, and Ar and appears to be a characteristic of the third-period atoms. The observation of the *KL* edge in Na, Mg, and Al is hampered by the experimental difficulties of building good monochromators to cover the range from 1000 to 1700 eV with sufficient energy resolution and smooth monochromatized flux. A suitable experiment, however, should reveal them easily.

In light of this extensive experimental evidence, gen-

eral trends of the *KL*-edge structure as a function of  $Z$  and ligands can now be drawn. A first striking experimental observation is that the overall shape of the *KL* edge is largely independent of the atomic number and molecular structure; indeed it is dominated by the presence of two main peaks, the second of greater intensity, separated by a few eV.

It is clear that the *KL*-edge shape is dominated by atomic effects justifying the use of a simplified atomic-level scheme in the assignment of the main features. As it has been already pointed out [20,13] the *KL*-edge peaks should be associated with the configuration  $1s2p(3p^*)^2$ , where  $3p^*$  represents the first available  $p$  resonance (that responsible for the *K*-edge ML). In this row of the Periodic Table relativistic effects can be neglected and hence the *LS* coupling scheme is appropriate. The previous four-particle configuration generates a complex multiplet structure containing three  $^1P$  states to which dipole transitions are allowed. With typical exchange and Coulomb integrals of third-period atoms the lower-lying resonance corresponds to a wave function in which the core holes are approximately coupled in a triplet configuration, referred to as the *T* peak. The second and third resonances correspond to wave functions in which the core holes are approximately coupled in a singlet configuration. Their separation with respect to the *T* peak is dominated by the hole-hole exchange interaction and amounts to about  $\frac{2}{3}G^1(1s, 2p)$  in terms of the Slater integrals. The second and third states are split by the smaller interactions between the  $1s$  or  $2p$  and  $3p^*$  orbitals which is of the order of  $\frac{1}{10}$  of the main splitting. With typical resolution and intrinsic Auger linewidths at this energy the two lines cannot be resolved and are likely to generate a single peak in the experimental spectra that will be referred to as the *S* peak. This simple model explains nicely the experimental observation of the two main peaks separated by a few eV that will be therefore indicated as *T* and *S* peaks, respectively. Notice that a possible splitting induced by ligand field effects, or spin-orbit interaction in the  $2p$  levels, can give rise to the slight distortions observed in some cases (in  $\text{CuSO}_4$ , for instance). The presence of the *T* and *S* peaks at the *KL* edge is a rather general occurrence that supports a picture in which the strongest features are dominated by atomic effects.

In order to make a comparison of the various measurements on a quantitative basis we report in a series of tables the relative energies and intensities of the *K*-edge ML and the *KL*-edge *T* and *S* resonances that were always observed.

#### A. Energies and splittings

The energies of the *K*-edge ML and those of the *T* and *S* peaks for all of the P, S, and Cl compounds together with the results for the  $\text{SiX}_4$  ( $X=\text{H}, \text{CH}_3, \text{Br}, \text{Cl}, \text{F}$ ) molecules are reported in Table I. The energies refer to the maximum of the corresponding peaks. The effect of asymmetries in the line shapes will be discussed in Sec. III B.

The energy difference between the *KL* edge and the *K*

TABLE I. Energy positions for the maxima of the *K*-edge ML and *T* and *S* resonances for the various compounds. In the last column the observed splitting between the *T* and *S* peaks is reported.

Compound	<i>K</i> -edge ML $E_0$ (eV)	Peak <i>T</i> $E_T$ (eV)	Peak <i>S</i> $E_S$ (eV)	<i>S</i> - <i>T</i> splitting (eV)
$\alpha$ -Si:H	1837.0(3)	1963.3(5)	1970.8(5)	7.2(5)
SiH <sub>4</sub>	1838.6(1)	1968.5(3)	1975.7(4)	7.2(5)
Si(CH <sub>3</sub> ) <sub>4</sub>	1839.6(1)	1969.8(1)	1977.4(1)	7.6(2)
SiBr <sub>4</sub>	1841.0(1)	1971.9(3)	1978.8(1)	6.9(3)
SiCl <sub>4</sub>	1841.9(1)	1973.4(1)	1980.3(1)	6.9(2)
SiF <sub>4</sub>	1844.7(1)	1980.0(1)	1986.8(1)	6.8(2)
Na <sub>2</sub> O:P <sub>2</sub> O <sub>5</sub>		2320.2(2)	2327.9(2)	7.7(3)
		2322.0(2)	2329.4(2)	7.4(3)
Na <sub>4</sub> P <sub>2</sub> O <sub>7</sub>		2321.5(3)	2329.1(2)	7.6(4)
NaH <sub>2</sub> PO <sub>4</sub>		2322.0(3)	2329.4(2)	7.4(4)
S	2471.7(1)	2668.3(3)	2678.6(3)	10.3(5)
Na <sub>2</sub> SO <sub>3</sub>	2478.2(1)	2681.7(5)	2690.2(3)	8.5(6)
Na <sub>2</sub> S <sub>2</sub> O <sub>6</sub>	2480.9(1)	2684.5(3)	2694.2(2)	9.7(4)
Na <sub>2</sub> S <sub>2</sub> O <sub>3</sub>	2480.8(1)	2685.4(5)	2694.2(2)	8.5(6)
K <sub>2</sub> SO <sub>4</sub>	2482.1(1)	2688.4(2)	2696.8(2)	8.4(3)
CuSO <sub>4</sub>	2482.4(1)	2689.0(3)	2697.6(2)	8.6(3)
NaClO <sub>2</sub>	2825.9(1)	3065.9(5)	3076.6(3)	10.7(6)
NaClO <sub>3</sub>	2830.2(1)	3073.6(5)	3083.6(2)	10.0(5)
NH <sub>4</sub> ClO <sub>4</sub>	2834.1(1)	3080.7(3)	3090.1(2)	9.4(4)

edge, that is, the extra energy required for the shake-up  $2p \rightarrow 3p$ , is as expected approximately constant for the different compounds of the same atom. The difference increases monotonically as a function of the atomic number being about 135 eV for Si, 213 eV for S, and 253 eV for Cl. This trend is clearly shown in Fig. 7 where the energy difference between the *S* peak position and the *K*-edge ML is plotted as a function of *Z*. The *S* peak has been chosen for practical purposes since it is better defined and more intense than the *T* peak. The same data for Ne and Ar as those reported in the Refs. [20,21] are included for completeness. Figure 7 also shows the binding energies of the  $2p$  electrons in the  $Z+1$  atom [25] (solid line) which are in excellent agreement with the experimental data. Even better agreement is obtained if differences of self-consistent atomic calculations for the configurations  $1s3p^*$  and  $1s2p(3p^*)^2$  are taken (dashed line). These calculations have been performed in the nonrelativistic, spin-averaged, and spherically averaged Hartree-Fock-Slater approximation for the free atom, using a computer code written by one of the authors [26]. The overall agreement between experimental points and curves means that the additional energy required to create the double hole and the charge-relaxation effects are correctly taken into account by either approximations. Clearly the success of the coarser  $Z+1$  approximation is due to the large separation of the charge densities among the various shells occurring in low-*Z* atoms. From the trends in Fig. 7, approximate energy predictions for the *KL* edge in Na, Mg, and Al can also be obtained.

Let us now discuss in some detail the general trends within the same atomic number that are evident from

Table I and the figures. The *K*-edge ML is due to the transition of the  $1s$  core orbital to the first available dipole-allowed state. This is the  $3p$  orbital in the case of Ne and the  $4p$  in the case of Ar. All of the Si, P, S, and

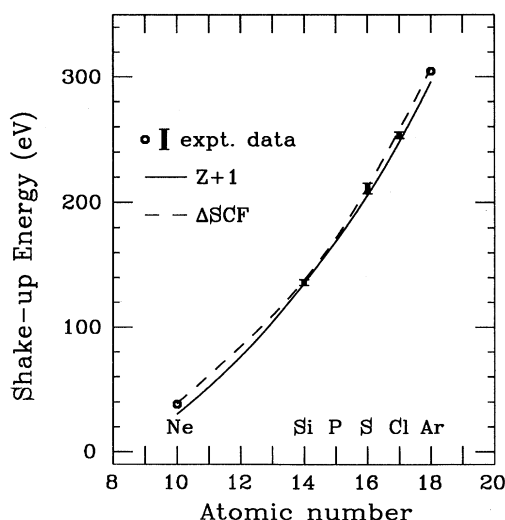


FIG. 7. Energy separation of *KL*-edge singlet peak (*S*) from the *K*-edge ML as a function of the atomic number. The circles indicate the experimental values for the noble gases while the vertical bars represent the energy range for the separation found in the various compounds of Si, S, and Cl. These data are compared with estimates in the  $Z+1$  approximation (solid line) and differences of self-consistent atomic calculations (dashed line).

Cl compounds are basically high-symmetry, closed-shell molecules. The  $3p$  orbitals of the photoabsorber atoms together with the ligand orbitals form a closed-shell bonding valence orbital and an empty antibonding orbital with a strong  $p$  character to which transitions can occur just like a  $3p$  orbital for the Ne case. This antibonding orbital, designated as  $3p^*$ , lies slightly in energy above the original  $3p$  orbital of the free atom. The effect of the electronegativity of the ligands is qualitatively explained as follows: with an increase of electronegativity (such as an increase in the number of oxygen atoms) the charge density of the valence orbitals shifts towards the ligand atoms and consequently the  $3p^*$  wave function collapses onto the photoabsorber atom increasing the dipole matrix element that determines the transition oscillator strength. At the same time the excitation energy increases due to the weaker screening by the valence electrons (chemical shift). Thus, for instance, the intensity of the ML in the Cl series ( $\text{NaClO}_2, \text{NaClO}_3, \text{NH}_4\text{ClO}_4$ ) increases by a factor of 2.4 and at the same time the ML energy shifts by about 8.2 eV.

It is interesting to note that the  $KL$ -edge resonances undergo a very similar behavior with even more dramatic effects. The intensities increase by a factor of 15 and the energy shift amounts to about 13.5 eV. This behavior can be qualitatively explained if the nature of the two resonance structures is considered. Indeed the multiplet structure observed at the  $KL$  edge is generated by the configuration  $1s2p(3p^*)^2$  in which two electrons are promoted to the  $3p^*$  antibonding orbital. The collapse of the  $3p^*$  wave function on increasing the oxidation state of the photoabsorber atom increases the dipole matrix element, but at the same time also increases the overlap  $\langle 2p|3p^* \rangle$  matrix element responsible through relaxation effects for the double-electron excitation. Thus the probability of double-electron excitations is strongly enhanced by the oxidation of the photoabsorber atom. At the same time the excitation energy of the  $KL$  edge reflects the chemical shift felt by both core electrons involved, and consequently a larger chemical shift than that of the  $K$  edge is expected.

The same trend of increased intensity and chemical shift with respect to the  $K$  edge has been observed in the case of S, Si, and to a minor extent in P where fewer compounds with a low oxidation state were available. Notice that in some of the S compounds ( $\text{Na}_2\text{S}_2\text{O}_3, \text{Na}_2\text{S}_2\text{O}_6$ ) the symmetry splitting of the antibonding molecular orbital gives rise to observable effects on the ML. This splitting [23] is, however, smaller than the singlet-triplet splitting at the  $KL$  edge and therefore the previous general discussion is still valid. In  $\text{Na}_2\text{S}_2\text{O}_3$  there are two nonequivalent S photoabsorbers: the central and the ligand S atoms in the  $\text{S}_2\text{O}_3^{2-}$  anion, with formal oxidation state of 6+ and 2-, respectively. These two atoms contribute to the absorption spectrum with two signals shifted like the elemental S and the  $\text{SO}_4^{2-}$  anion spectra. In fact, the  $\text{Na}_2\text{S}_2\text{O}_3$   $K$ -edge spectrum reveals the presence of two sharp edge resonances corresponding to the two oxidation states (see also Ref. [23]). In the corresponding  $KL$ -edge spectrum it is the  $\text{S}^{6+}$  which provides the larger resonances because of the oxidation effect on the cross sec-

tion and the  $\text{S}^{2-}$  atom generates only weaker features.

A comprehensive plot that correlates the  $K$ -edge ML shift with that of the  $KL$ -edge resonances in the case of Si, S, and Cl compounds is shown in Fig. 8. The  $K$ -edge ML energy positions on the  $X$  axis are reported on a relative energy scale. On the  $Y$  axis the energy positions of  $KL$ -edge resonances is reported with similar criteria. For each of the measured compounds, there are two corresponding "experimental" points, one for each resonance line. The points corresponding to the same resonance line ( $S$  or  $T$ ) of different compounds of the same photoabsorber atom are joined by solid lines for clarity. For each of the three elements Si, S, and Cl there correspond two almost-parallel lines describing the correlation between  $K$ -edge and  $KL$ -edge shifts. The positions of the data corresponding to different atoms is arbitrary due to the relative energy scales, but the slopes of the lines can be directly compared. The general trends shown in Fig. 8 are consistent with the observation that the chemical shift at the  $KL$  edge is about 1.7 times that of the  $K$  edge. Small deviations from straight lines indicate a small dependence of the actual chemical shift on the compound under consideration, but the general trend is evident from Fig. 8. The results reported in Fig. 8 might have interesting applications; indeed the  $KL$  edge is associated with shake-up channels that in principle should be observed in the corresponding x-ray photoemission spectroscopy spectra. These shake-up peaks will manifest a larger chemical shift with respect to the  $1s$  core peak and therefore their observation should allow a more precise chemi-

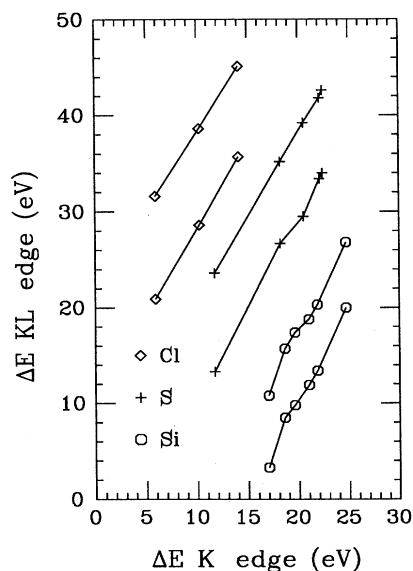


FIG. 8. Correlation of the chemical shift at the  $KL$  edge with that of the  $K$  edge for several compounds of the elements Si, S, and Cl. The energy of the  $T$  (lower) and  $S$  (upper) resonances at the  $KL$  edge is reported on the  $y$  axis as a function of the  $K$ -edge ML energy ( $x$  axis). The origins are shifted for graphical purposes and correspond to (1820,1960) for Si, (2460,2655) for S, and (2820,3045) for Cl. Notice the general linear behavior of the  $KL$ -edge shift that is about 1.6–1.7 times the  $K$ -edge one.

cal characterization of the compound. Obviously this larger sensitivity is paid for by the larger experimental difficulties due to the smaller intensity, but with a modern photoemission apparatus it should not be difficult to obtain suitable spectra.

Let us now turn to the problem of *KL*-edge energy splitting trends versus atomic number *Z*. In the last column of Table I the splitting between the two lines *S* and *T* is reported and is seen to monotonically increase from Ne to Ar. This trend is summarized in Fig. 9 where the splitting is reported as a function of the atomic number. For each element the splitting observed in the various compounds is reported. Notice that there are slight differences among different compounds of the same absorbing atom for all Si, P, S, and Cl cases, which have been discussed previously. In general the splitting seems to reach the lower magnitude in the compound with the maximum possible oxidation state. The high-oxidation-state data are nicely aligned with the noble-gases splitting, dashed line in Fig. 9, but this occurrence apparently does not have a simple explanation.

The general trend of increasing splitting as a function of *Z* is easily explained according to the common interpretation that it is dominated by the singlet-triplet splitting of the core hole that amounts to  $\frac{2}{3}G^1(1s,2p)$  in terms of the exchange Slater integrals. The *G* integral should be evaluated for the atom in the final-state configuration, and accurate self-consistent calculations performed. The theoretical splittings have been calculated for the different atoms and the linear trend is seen as the solid

line in Fig. 9. The theoretical splitting is in general larger than that seen in the experimental data apart from some high splitting values observed in a few low-oxidation-state compounds. In particular it is larger than the highest oxidation limit shown as a dashed line in Fig. 8. In order to match the dashed line, the  $G^1(1s,2p)$  integral should be reduced by 31% in the limiting case of Ne and by 9% in the Ar case. The discrepancy is explained by the presence of correlation effects which, as is well known, reduce the bare Coulomb interactions between electrons [27]. The experimental evidence supports the presence of correlation effects providing a larger reduction factor in the case of a lower-*Z* atom which is expected because of the larger weight of a single electron with respect to the full atomic charge. Some of this correlation can actually be taken into account, including the effects of the spin polarization of the Hamiltonian in the self-consistent potential. The differences of total energy calculation performed in a spin-dependent spherically averaged Hartree-Fock scheme [26], for triplet and singlet configurations of the type  $1s2p(3p^*)^2$ , are reported as crosses and are joined by a dotted line in Fig. 9. At least for the Si, P, S, and Cl atoms these splitting values are in slightly better agreement with the experiments than the  $\frac{2}{3}G^1(1s,2p)$  values.

## B. Intensities and line shapes

Let us now discuss the trends in peak intensities and line shapes. There are two evident features common to all of the experimental spectra: the *KL*-edge resonances have asymmetric line shapes due to autoionization processes and the *T*:*S* peak-intensity ratio is about 1:2 throughout *Z*=14–17. This apparent intensity ratio may be affected by the line shape itself and in order to make quantitative statements it is necessary to perform fits of the spectra using appropriate profiles.

In the framework of the present investigation we attempted to model the experimental spectra by using the sum of a certain number of independent resonance lines according to the Beutler-Fano [18] profiles. The main limitation of this model is that the three predicted  $^1P$  terms corresponding to the  $1s2p(3p^*)^2$  configuration and possible additional resonances associated with higher excited configurations may be strongly interacting among themselves through the coupling with several continua. Notice that the observed resonances do not belong to a Rydberg series, a case which has been widely discussed [18], and represent an interesting example of autoionization effects.

As has been pointed out, the general case of several resonances interacting with several continua presents a complex phenomenology with a large number of unknown parameters [29] and the information contained in the absorption spectrum alone may be not sufficient to uniquely characterize the observed resonances. Besides, a fitting procedure is also affected by several experimental uncertainties that require further investigation. The first is the exact composition of the multiplet structure and the possible effect of the successive resonances associated with different configurations that, even assuming perfect

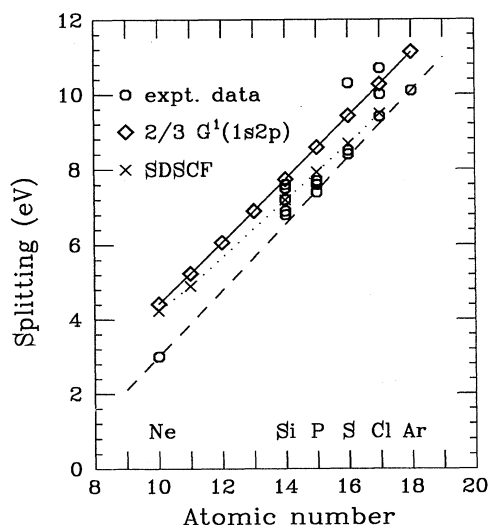


FIG. 9. Splitting of the *T* and *S* resonances as a function of the atomic number. The experimental data, reported as small circles, show a linear behavior. In particular the data relative to the  $\text{SiF}_4$ ,  $\text{NaH}_2\text{PO}_4$ ,  $\text{K}_2\text{SO}_4$ , and  $\text{NH}_4\text{ClO}_4$  compounds are aligned with the noble-gases data (dashed line). The theoretical data for the splittings are indicated with  $\diamond$  and are joined by a solid line. Notice the reduction of the *G* integral that is needed to explain the experimental data due to correlation effects.



separation, will affect the background on the right-hand side of the peak *S*. The second is the presence of the slowly varying *K*-edge EXAFS oscillation providing an oscillating background smoother than the *KL*-edge multiplet structure.

With these limitations in mind, we performed fits of the spectra in some representative cases. The model spectra were obtained by adding to a third-degree polynomial background, accounting for the *K*-edge contribution, a certain number of resonance lines according to the following parametrization of the Beutler-Fano line shapes;

$$\sigma(E) = \frac{\sigma_{\Phi}}{\pi\Gamma(1+\eta^2)}(1-r^2+2r\eta), \quad (1)$$

where  $\sigma_{\Phi}$  represents the cross section to the bound autoionizing state,  $\eta = (E - E_r)/\Gamma$  is the reduced energy distance from the resonance energy  $E_r$ ,  $\Gamma$  is the half width at half maximum of the line, and finally the asymmetry parameter  $r = 1/q$  is the inverse of the Fano parameter  $q$  and is proportional to the coupling with the continuum and to the transition matrix elements involving the initial state and continuum final state as well as the initial state and discrete final state. In the limit  $r = 0$  the line reduces to a Lorentzian shape.

Each of the main *KL*-edge resonances, in particular both the *T* and *S* peaks, were modeled by a single line according to Eq. (1). This hypothesis provides correct Fano parameters if three resonances were not interacting, and if the third unobserved <sup>1</sup>*P* resonance is very weak or if it is degenerate in energy and has a shape similar to the other one associated with the *S* peak. In the latter case the intensity parameter will represent the sum of the two intensities. Moreover, one or two other peaks were added at higher energies to account for the smaller resonances that are often visible. This was done simply to account for the background on the right-hand side of peak *S* and no specific assignment has been yet attributed to these parameters. The model spectra were convolved

with a Gaussian representing the monochromator resolution and fit to the experimental spectra minimizing the sum of the square differences between them.

In the same way a fit of the ML corresponding to the  $1s \rightarrow 3p^*$  transition at the *K* edge was also performed for each sample in order to obtain the intensity of the one-electron resonance. In this case the  $r$  parameter in (1) was set to 0.

The results of the fits provide estimates for widths, asymmetries, and intensities of the various peaks. The lifetime full width at half maximum (FWHM) of the ML is a known parameter ranging from about 0.48 eV for Si to 0.64 eV for Cl [28]. In order to reproduce the experimental ML the additional resolution broadening was necessary. Gaussian standard deviations in the range 0.3–0.6 eV were found according to the edge and monochromator used. The first significant result on the *KL*-edge resonances is that the  $\Gamma$  parameter for the *S* and *T* peaks were found to be significantly larger than the corresponding ML lifetime widths. The total widths (FWHM) where  $2\Gamma = 2.7(3)$  eV for  $\text{SiCl}_4$  and in the range 3.2–4.5 eV for the other compounds. This is naturally attributed to the reduced lifetime due to the autoionizing decay of the resonances. Within the accuracy of the fits it is not possible to identify clear trends versus atomic number or compound, but we can certainly provide an estimate for the autoionizing width of these resonances. Notice that according to Mies (see Fig. 1 of Ref. [29]), in the interacting case, these values can represent lower limits of the real autoionizing widths. In Table II we report, for six representative samples, the intensity *I* and asymmetry parameters for the ML and for the *T* and *S* peaks, respectively. The inverse of the  $q$  Fano parameters are reported in columns 4 and 6 for the *T* and *S* peaks, respectively. Although the numbers are not exactly identical for the various compounds we can make some general observations. Both resonances have negative  $q$  values which provides a constraint to the signs of the three matrix elements occurring in its definition. The  $1/q$  values are found in the range  $-0.5$  to  $-0.8$  for the *T* peak, com-

TABLE II. Intensities and asymmetries of the main resonance lines for a representative set of compounds indicated in column 1. The intensities *A* of the ML and of the *T* and *S* peaks are reported in columns 2, 3 and 5, respectively, in *J* eV units (see text). The  $1/q$  Fano parameters are reported in columns 4 and 6 for the *T* and *S* peaks, respectively. Column 7 contains the dimensionless ratio between the total intensity of the *KL* multiplet ( $I_T + I_S$ ) and the ML intensity. The last column contains the *T*:*S* peak intensity ratio.

Compound	ML	<i>T</i> peak		<i>S</i> peak		$\frac{I_T + I_S}{I_{ML}}$	$\frac{I_T}{I_S}$
	<i>I</i> <sub>ML</sub> ( <i>J</i> eV)	<i>I</i> <sub><i>T</i></sub> ( <i>J</i> eV)	$1/q$	<i>I</i> <sub><i>S</i></sub> ( <i>J</i> eV)	$1/q$		
$\text{SiCl}_4$	13.3(3)	0.04(1)	−0.5(2)	0.18(2)	−0.4(1)	0.016(2)	0.2(1)
$\text{NaH}_2\text{PO}_4$		0.022(8)	−0.8(2)	0.07(2)	−0.4(1)		0.3(1)
$\text{K}_2\text{SO}_4$	13.3(6)	0.044(5)	−0.5(1)	0.11(1)	−0.4(1)	0.011(2)	0.4(1)
$\text{NaClO}_2$	8.9(5)	0.005(2)	−0.8(2)	0.021(5)	−0.4(2)	0.003(1)	0.2(1)
$\text{NaClO}_3$	13.6(6)	0.038(5)	−0.7(1)	0.054(8)	−0.3(1)	0.007(1)	0.7(2)
$\text{NH}_4\text{ClO}_4$	21(2)	0.077(8)	−0.8(1)	0.27(3)	−0.3(1)	0.016(3)	0.3(1)

pared to the range  $1/q \approx -0.3$  to  $-0.4$  for the  $S$  peak. Thus the apparent asymmetries are different and in general the  $T$  peak is found to be more asymmetric than the  $S$  one. Of course this might be an artifact of the presence of the two closely spaced  $^1P$  resonances. These results provide preliminary estimates for the autoionization parameters and are given here to suggest guidelines for future experiments or calculations. A conclusive statement on the level of interaction among the resonances and exact line shape will require further investigations.

Finally we wish to discuss the intensity results reported in columns 2, 3, and 5 of Table II and the dimensionless ratios reported in the last two columns. The energies have been measured in eV while the absorption unit was taken as the  $K$ -edge jump ( $J$  defined in Sec. II C). This was measured easily with a full  $K$ -edge scan of the same sample and allows one to get an absolute value for the cross section provided that an absolute determination of the jump cross section is performed. The units of the peak intensities are the jump units times the width in eV ( $J$  eV). The estimated error of the ML intensity (reported in Table II), due to the noise of the signal, is only a few percent. The intensity measurements may be affected, however, by more serious systematic errors due to the sample inhomogeneities and self-absorption that may considerably reduce the height of the ML peak. This signal reduction, which is hard to estimate, should, however, be limited to a maximum of about 20% due to the careful sample-preparation technique. The intensity of the  $KL$ -edge peaks was given directly by  $\sigma_\phi$  in Eq. (1). The error of these intensity estimates ranges from the 5% in the best case to the 30% in the worst. The main sources of error are, besides the experimental noise, the uncertainty in the background shape as discussed above, the presence of contamination peaks (like in  $\text{NaClO}_2$ ), and the uncertainty arising from the hypotheses about their composition.

In column 7 of Table II the dimensionless ratio between the total  $T+S$  intensity and the ML intensity  $I_{\text{ML}}$  is reported. It is evident that the overall intensity of the  $KL$ -edge resonances with respect to the  $K$ -edge ones is strongly compound dependent. For instance, in the  $\text{ClO}_n$  series the ratio ranges from 0.3% to 1.6%, which means that the absolute strength increases by a factor of about 15, clearly observable in Fig. 2. This is much higher than the corresponding increase of the ML intensity which is only of a factor 2.4.

The  $(I_T + I_S)/I_{\text{ML}}$  ratio is a quantity independent of the possible rearrangement of the oscillator strengths within the multiplet and is given by the ratio of the squared transition matrix elements  $A_K$  and  $A_{KL}$  associated with the  $K$  and  $KL$  edges, respectively. Considering only the dominant contributions in the matrix elements these are simply given by

$$A_K \approx \langle 1s | \hat{\epsilon} \cdot \mathbf{r} | 3p_K^* \rangle, \quad (2)$$

$$A_{KL} \approx \langle 1s | \hat{\epsilon} \cdot \mathbf{r} | 3p_{KL}^* \rangle \langle 2p | 3p_{KL}^* \rangle, \quad (3)$$

where  $\hat{\epsilon}$  is the photon polarization vector. The final state  $3p^*$  orbitals are in principle different because of the different charge relaxation in the two cases. The dimensionless ratio is given by

dimensionless ratio is given by

$$\frac{I_T + I_S}{I_{\text{ML}}} = \frac{10 A_{KL}^2}{2 A_K^2} \approx 5 \langle 2p | 3p^* \rangle^2, \quad (4)$$

where  $A_{KL}$  and  $A_K$  are defined above and the numerical factors derive from the spin and angular momentum degeneracies. The last approximate equality is obtained in the limit of considering equal the dipole matrix elements, i.e., if the differences of the  $3p^*$  orbital at the  $K$  and  $KL$  edges are neglected. By applying the approximate result of Eq. (4) to the experimental data it is possible to estimate the modulus of the overlaps  $\langle 2p | 3p^* \rangle$ . They are in the range 0.024–0.057, the largest values occurring when the photoabsorber element is combined with highly electronegative atoms.

The  $T:S$  ratio, reported in the last column, is connected with the distribution of the oscillator strength among the multiplet peaks and in particular between the triplet- and singlet-type configurations. The  $T:S$  ratio shows some variations among the different compounds around an average value of about 0.4. The apparent intensity of the  $T$  resonance is actually magnified by the asymmetry of the peak which is larger than that of the  $S$  peak. As a consequence the apparent peak height ratio is about 1:2.

The  $T:S$  ratio can be predicted in the  $LS$  coupling scheme starting from a set of basis wave functions obtained in a spherically averaged and spin-averaged potential. In the limit of dominant  $1s$ - $2p$  interaction the theoretical ratio is found to be  $T:S=6:4$  [30]. The account of the smaller  $1s$ - $3p$  and  $2p$ - $3p$  interactions provides only a slight correction to this value. This result is clearly in disagreement with the experimental findings of a ratio approximately equal to 0.4 and suggests that correlation effects produce a transfer of oscillator strength from the  $T$  to the  $S$  peak. The observed ratio can be calculated with reasonable accuracy starting from a different zero-order approximation that takes immediately into account the spin polarization of the electronic-charge density upon core excitation. It can be shown [30] that a spherically averaged spin-dependent Hartree-Fock calculation for the  $1s(\uparrow)2p(\uparrow)[3p^*(\uparrow)]^2$  ( $T$  type) and  $1s(\uparrow)2p(\downarrow)3p^*(\uparrow)3p^*(\downarrow)$  ( $S$  type) configurations provides, besides the correct splitting mentioned above, also a reversed intensity ratio between the  $T$  and  $S$  components. In particular the numerical degeneracies are in a ratio 4:6, with additional reduction of the  $T:S$  ratio arising from matrix-elements effects because the  $3p^*$  wave functions are slightly different in the  $T$  and  $S$  cases resulting in a noticeable variation of overlap matrix elements.

#### IV. CONCLUSION

A comprehensive account of the available experimental data on  $KL$ -edge resonances in x-ray absorption spectra of third-period atoms has been provided. The presence of two well-defined peaks split by the hole-hole exchange interaction with an apparent intensity ratio of about 1:2 seems to be a rather common characteristic of these edges. Very similar shapes are indeed found in several compounds of Si, P, S, and Cl. Their presence is rather general and depends weakly on the ligands, which, however, affect the overall intensity and produce chemical

shifts (in addition to those caused by the oxidation state of the absorber). A certain number of quantitative conclusions can be drawn. The additional shake-up energy required to create the double excitation as a function of the atomic number increases in agreement with the prediction of self-consistent calculations. The chemical shift occurring at the *KL* edge is found to be about 1.7 times the corresponding *K*-edge shift. The splitting between the *T* and *S* peaks increases almost linearly as a function of the atomic number as expected from the trend of the  $G^1(1s,2p)$  integral. Significant reduction of the actual splitting magnitude which can be attributed to correlation effects is found. The *T* and *S* peaks have autoionization profiles that when analyzed using an independent resonance model provide additional widths in the range 2.7–4.5 eV. The inverses of the Fano *q* parameter are found in the range  $-0.5$  to  $-0.8$  for the *T* peak and  $-0.3$  to  $-0.4$  for the *S* peak. The overall intensity of the *KL*-edge multiplet (*T* + *S*) peak depends strongly on the electronegativity of the ligands; differences of more than one order of magnitude have been found in the  $\text{ClO}_n$  series. These intensity ratios can be reproduced with typical overlap matrix elements with magnitudes in the range 0.024–0.057. The *T*:*S* = 6:4 intensity ratio predicted using an *LS*-coupling scheme starting from a spin- and spherically averaged self-consistent calculation in the lim-

it of dominant  $G^1(1s,2p)$  interaction is in disagreement with the experimental observation. The importance of correlation effects in determining the final shape of the  $1s2p(3p^*)^2$  autoionizing resonances in third-period atoms is addressed.

#### ACKNOWLEDGMENTS

The authors would like to acknowledge Dr. P. Frank (Stanford University, Chemistry Department) and Dr. B. Hedman (Stanford Synchrotron Radiation Laboratory) for assistance in carrying out the measurements done at Stanford. Thanks are due to the staff of the "Gruppo PULS" LNF Frascati, in particular to F. Campolungo for skillful technical assistance, and to Dr. A. Di Cicco (Università di Camerino) for helpful discussions. This work was supported by National Science Foundation Grant No. CHE 91-21576 (K.O.H.). The operation of the Stanford Synchrotron Radiation Laboratory is supported by the Department of Energy (DOE), Office of Basic Energy Sciences, Divisions of Chemical and Material Sciences, and further support is provided by NIH (Grant No. RR01209) and the DOE Office of Health and Environmental Research. T.A.T. acknowledges support from the Stanford School of Humanities and Sciences and the Dean of Research.

- [1] F. Wuilleumier, C. R. Acad. Sci. Paris **263**, 450 (1966).
- [2] H. W. Schnopper, Phys. Rev. **131**, 2558 (1963).
- [3] R. D. Deslattes, R. E. LaVilla, P. L. Cowan, and A. Henins, Phys. Rev. A **27**, 923 (1983).
- [4] G. B. Armen, T. Åberg, K. R. Karim, J. C. Levin, B. Crasemann, G. S. Brown, M. H. Chen, and G. E. Ice, Phys. Rev. Lett. **54**, 182 (1985).
- [5] M. Deutsch and M. Hart, Phys. Rev. A **34**, 5168 (1986).
- [6] E. Bernieri and E. Burattini, Phys. Rev. A **35**, 3322 (1987).
- [7] Y. Ito, H. Nakamatsu, T. Mukoyama, K. Omote, S. Yoshikado, M. Takahashi, and M. Emura, Phys. Rev. A **46**, 6083 (1992).
- [8] P. D'Angelo, A. DiCicco, A. Filipponi, and N. V. Pavel, Phys. Rev. A **47**, 2055 (1993).
- [9] K. Zhang, E. A. Stern, J. J. Rehr, and F. Ellis, Phys. Rev. B **44**, 2030 (1991).
- [10] M. Deutsch and P. Kitzler, Phys. Rev. A **45**, 2112 (1992).
- [11] T. M. Hayes and J. B. Boyce, in *Solid State Physics*, edited by H. Ehrenreich, F. Seitz, and D. Turnbull (Academic, New York, 1982), Vol. 37, p. 173. P. A. Lee, P. Citrin, P. Eisenberger, and B. Kincaid, Rev. Mod. Phys. **53**, 769 (1981).
- [12] A. Balerna, M. Benfatto, S. Mobilio, C. R. Natoli, A. Filipponi, and F. Evangelisti, J. Phys. (Paris) Colloq. **8**, C-63 (1986); A. Filipponi, E. Bernieri, and S. Mobilio, Phys. Rev. B **38**, 3298 (1988).
- [13] S. Bodeur, P. Millie, E. Lizon à Lugrin, I. Nenner, A. Filipponi, F. Boscherini, and S. Mobilio, Phys. Rev. A **39**, 5075 (1989).
- [14] A. Di Cicco, S. Stizza, A. Filipponi, F. Boscherini, and S. Mobilio, J. Phys. B **25**, 2309 (1992).
- [15] J. Chaboy, J. García, A. Marcelli, and M. F. Ruiz-López, Chem. Phys. Lett. **174**, 389 (1990).
- [16] E. Dartyge, A. Fontaine, Ch. Giorgetti, S. Pizzini, F. Baudelet, G. Krill, Ch. Brouder, and J.-P. Kappler, Phys. Rev. B **46**, 3155 (1992).
- [17] G. Li, F. Bridges, and G. S. Brown, Phys. Rev. Lett. **68**, 1609 (1992).
- [18] U. Fano, Phys. Rev. **124**, 1866 (1961).
- [19] R. P. Madden and K. Codling, Phys. Rev. Lett. **10**, 516 (1963).
- [20] J. M. Esteve, B. Gauthé, P. Dhez, and R. C. Karnatak, J. Phys. B **16**, L263 (1983).
- [21] U. Kuetgens and J. Hormes, Phys. Rev. A **44**, 264 (1991).
- [22] A. Kodre, M. Hribar, I. Arčon, D. Glavič-Cindro, M. Štuhec, R. Frahm, and W. Drube, Phys. Rev. A **45**, 4682 (1992).
- [23] T. A. Tyson, A. L. Roe, P. Frank, K. O. Hodgson, and B. Hedman, Phys. Rev. B **39**, 6305 (1989).
- [24] J. L. Dehmer and D. Dill, J. Chem. Phys. **65**, 5327 (1976).
- [25] *Photoemission in Solids I: General Principles*, edited by M. Cardona and L. Lay (Springer-Verlag, Berlin, 1978).
- [26] A. Filipponi (unpublished).
- [27] I. Lindgren and J. Morrison, *Atomic Many-Body Theory* (Springer-Verlag, Berlin, 1982), p. 311.
- [28] M. O. Krause and J. H. Oliver, J. Chem. Ref. Data **8**, 329 (1979).
- [29] F. H. Mies, Phys. Rev. **175**, 164 (1968).
- [30] A. Filipponi and T. A. Tyson (unpublished).